International Conference on Space Optics—ICSO 2014

La Caleta, Tenerife, Canary Islands

7–10 October 2014

Fast-steering solutions for cubesat-scale optical communications

R. W. Kingsbury

T. Nguyen

K. Riesing

K. Cahoy

FAST-STEERING SOLUTIONS FOR CUBESAT-SCALE
OPTICAL COMMUNICATIONS

R. W. Kingsbury, T. Nguyen, K. Riesing, K. Cahoy

MIT Space Systems Laboratory, Massachusetts Institute of Technology, United States of America

77 Massachusetts Avenue, Cambridge, MA 02139, U.S.A.

kingryan@mit.edu

I. INTRODUCTION

We describe the design of a compact free-space optical communications module for use on a nanosatellite and present results from a detailed trade study to select an optical fine steering mechanism compatible with our stringent size, weight and power (SWaP) constraints. This mechanism is an integral component of the compact free-space optical communications system that is under development at the MIT Space Systems Laboratory [1]. The overall goal of this project is to develop a laser communications (lasercom) payload that fits within the SWaP constraints of a typical "3U" CubeSat. The SWaP constraints for the entire lasercom payload are $5\,cm \times 10\,cm \times 10\,cm$, 600 g and 10 W. Although other efforts are underway to qualify MEMS deformable mirrors for use in CubeSats [2], there has been very little work towards qualifying tip-tilt MEMS mirrors [3].

Sec. II provides additional information on how the fast steering mechanism is used in our lasercom system. Performance requirements and desirable traits of the mechanism are given. In Sec. III we describe the various types of compact tip-tilt mirrors that are commercially available as well as the justification for selecting a MEMS-based device for our application. Sec. IV presents an analysis of the device's transfer function characteristics and ways of predicting this behavior that are suitable for use in the control processor. This analysis is based upon manufacturer-provided test data which was collected at standard room conditions. In the final section, we describe on-going work to build a testbed that will be used to measure device performance in a thermal chamber.

II. MOTIVATION AND DESIGN OVERVIEW OF A CUBESAT-SCALE LASERCOM MODULE

Many free-space optical communication system designs over the past decade have targeted deep-space missions which demand extremely precise pointing. Microradian beam widths are common in these applications in order to achieve high data rates over long path lengths. Our design is intended for use on CubeSats which are generally deployed in low earth orbit (LEO). Path lengths for LEO-to-ground operations are many orders of magnitude less than deep-space lasercom systems.

Shorter path lengths (1000 km max for our system) allow for the use of wider beamwidths (e.g. 2.1 **milli**radian) than deep-space applications (**micro**radians). Widening the transmit optical beam simplifies beam pointing while still providing a significant advantage over radio frequency (RF) communication alternatives. Other notable demonstrations of CubeSat-scale lasercom, such as AeroCube-OCSD [4], are predicted to achieve sufficient pointing performance (1.7 mrad) simply by body-pointing the entire spacecraft. This is a reasonable approach for a CubeSat due to the agility of the vehicle (low moments of inertia) and the very broad beam widths (5 mrad) but the single-stage control approach may limit the advantage of lasercom over RF systems. Multi-stage control systems, which can simultaneously provide good range, resolution and bandwidth, are the norm in most lasercom systems.

Pointing improvements are one of the key "enablers" for scaling lasercom implementations to higher data rates. Our project seeks to implement a two-stage control system that can evolve to provide data rates exceeding 100 Mbps while keeping power consumption below a self-imposed limit of 10 W. In our design, the host spacecraft still provides coarse pointing and the high-rate slew maneuver ($1\,^{\circ}\,s^{-1}$) that is needed to track the ground station. The coarse stage is supplemented by a fine stage, which has a limited field of regard but much better precision and bandwidth. An uplink beacon signal provides the pointing knowledge which is used to adjust the steering of the downlink signal.

A bistatic optical design, consisting of separate transmit and receive optical paths, has been selected for this application (Fig. 1). This approach simplifies the design of each path since it allows them to be optimized independently.
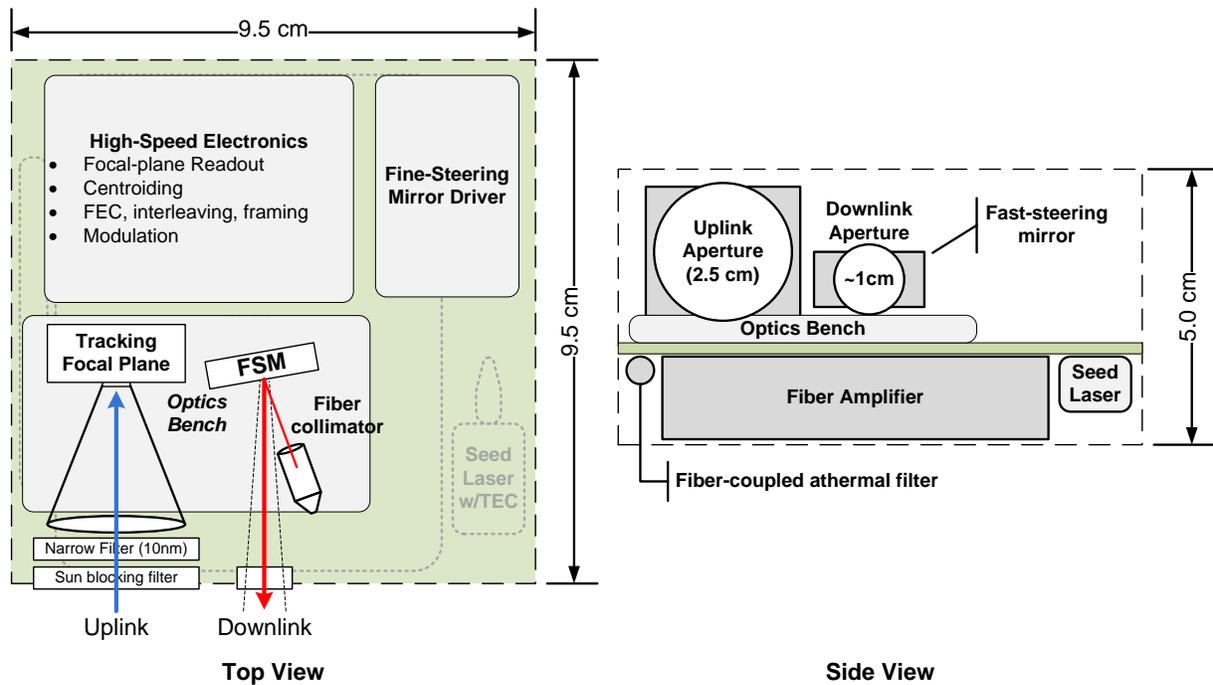
Fig. 1: *Layout diagram of the CubeSat-scale lasercom payload*

The main engineering cost of the bistatic approach is the need to ensure alignment between the two systems as well as on-orbit calibration methods. This approach would not be suitable for deep-space lasercom systems due to alignment challenges, but our relatively generous 2.1 mrad beamwidth make this problem much more tractable.

We have selected a 2.5 cm aperture for the uplink signal (driven by photon collection needs of the beacon detector) and a much smaller (millimeter-scale) downlink aperture which is sufficient for achieving the desired 2.1 mrad beamwidth. The downlink fine-steering architecture is a "gimbaled" flat design consisting of a fiber beam coupler (which establishes the desired beam divergence) and a fast-steering mirror. The requirements for the fast-steering mirror are summarized in Table 1.

Table 1: *Fine control stage requirements & design goals*

Parameter	Value	Justification / Driver
Actuation Type	2-axis (tip/tilt)	Insufficient space for two single-axis devices
Field of regard	± 17.0 mrad	Post-acquisition coarse-stage accuracy plus margin
Accuracy	± 0.11 mrad	1/20th of downlink beamwidth
Bandwidth	> 10 Hz	Rate of control loop (detector readout limited)
Diameter	> 2 mm	Mechanical alignment
Size goal	$< 2\,\text{cm} \times 2\,\text{cm} \times 2\,\text{cm}$	Including driver electronics
Mass goal	< 100 g	Including driver electronics
Power goal	< 100 mW	While steering at full bandwidth

III.   Fast-Steering Mechanism Trade Study

At the beginning of this project, three different FSM types were considered for use. These can be grouped by their actuation type: mechanical, piezoelectric, and microelectromechanical (MEMS) devices.

Conventional mechanical FSMs, which typically use voice coils for actuation, were eliminated early in the project due to their inability to meet size constraints. Many devices in this category, such as the Newport FSM-300, provide large mirrors (e.g. 25.4 mm) which are unnecessary for our application. These products also have large moving masses which make them more susceptible to shock and vibration damage. Voice coils, which are current-driven, also tend to have high power consumption (some manufacturers quote figures > 1 W). This also exceeds our requirements. Finally, our group's prior experiences with designing and qualifying mechanical actuators for CubeSats has given us a healthy respect for amount of engineering time required to qualify a mechanical actuator [5].

Piezoelectric mirrors, such as the Physik Instrumente (PI) S-334, were also considered for this application. The PI S-334 offers sufficient steering range and precision for our application. Unfortunately, the underlying piezoelectric actuation technology exhibits strong non-linearity and hysteresis which requires the use of a complex closed-loop controller. Although the S-334 mirror fits roughly within our SWaP constraints, the smallest available controller (PI E-616) does not (19 cm × 13 cm × 10 cm, 950 g, 30 W). It is likely that this controller could be miniaturized for use in our application, however, this too would require a significant engineering effort.

The third class of devices that were considered were MEMS tip-tilt mirrors. This category of devices can further be divided into electrostatic and electromagnetic actuation styles. The Texas Instruments TALP1000B is an example of a electromagnetically actuated MEMS FSM. This FSM and driver circuit meet our SWaP requirements as described in [6]. Unfortunately this device is no longer in production, thus it was eliminated from the study.

The second type of MEMS FSMs are electrostatically actuated. A wide variety of electrostatic MEMS FSMs are available from Mirrorcle Technology Inc (MTI). These chip-scale (0.5 cm × 0.5 cm × 0.1 cm) devices have steering ranges exceeding ±20 mrad and are available with low-SWaP driver boards. The mirrors options range from 1 mm to 6 mm in diameter, large enough for our application. These devices do not incorporate built-in position sensors (which could be used for closed-loop control) but have well-behaved transfer functions that allow most users to operate them in an open-loop configuration. These devices were selected for further development due to their highly favorable SWaP. The remainder of this paper discusses the analysis and qualification of a Mirrorcle Technology 13L2.2 actuator factory-fitted with a 2.4 mm diameter mirror.

IV.   Characterization of MEMS Fast Steering Mirror for Lasercom

In this section we analyze the performance of the MEMS FSM and present methods under consideration for determining the proper drive voltages needed to achieve a desired steering angle. Since we will be operating the mirror in an open-loop configuration, the driver will need to be capable of compensating for any known non-linearity of the FSM. The analysis that follows is based upon manufacturer-collected test data that is included with each device [7]. This data has been collected at standard room temperature and pressure.

The device under consideration is an MTI 13L2.2 fitted with a 2.4 mm mirror. This device has approximately a ±21.8 mrad steering range in both axes. Fig. 2 shows the single axis transfer functions for the FSM (generated from [7]). The curves in Fig. 2 are predominantly linear, so our first approach was to least-squares fit a linear function to the measured data. The purpose was to determine if the residual error between this linear fit and the measured data was within the ±0.11 mrad accuracy requirement. The error between this linear mirror model and the measured data is plotted in Fig. 3 for the x-axis of the device. Clearly, the accuracy requirement is not met using this simplistic approach. The FSM response cannot be treated as linear.

A 5th order polynomial provides a much-improved least-squares fit for the data as seen in the red trace in Fig. 3. The same approach can be applied to the y-axis transfer function with similar results. We do note that the data which this is based upon is quite "noisy." The manufacturer believes that this noise is an artifact of their measurement technique and not of the mirror itself. This is one issue we plan to investigate further in our FSM measurement testbed.

The single-axis models just described do not account for mechanical coupling that occurs between the two axes. Nevertheless, the two single-axis models can be used together and compared against measurement data that covers
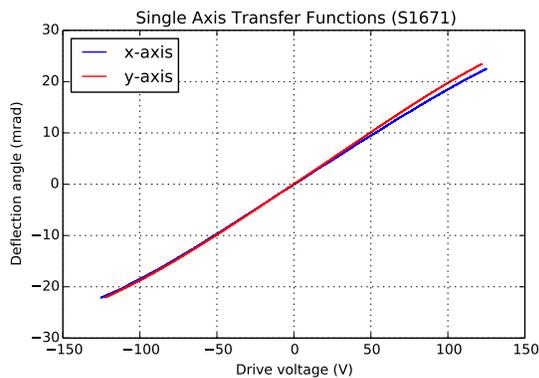
Fig. 2: *Representative transfer function for MEMS FSM showing two full "out and back" sweeps of device's range.*
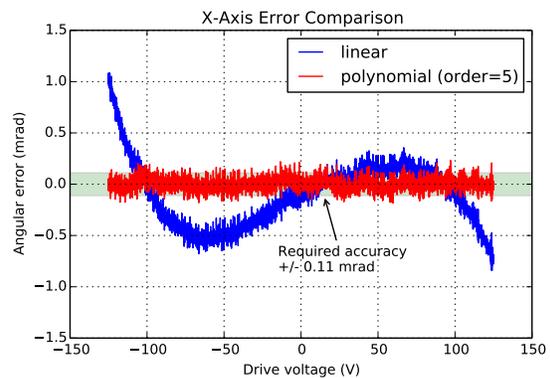
Fig. 3: *Comparison of fit for linear and 5th order polynomial models for the x-axis.*

the entire range of the device. The result of this comparison is shown in Fig. 4, the red contour line shows the required performance threshold (± 0.11 mrad). Performance is generally poorer in the corners where both axes are near their maximum deflection angles. Increasing the order of the underlying single-axis polynomials does not improve performance.

Because of the 2D nonuniformities of the FSM, it will likely be necessary to interpolate a 2D look-up table to linearize the device. The size of this table is a topic for future research. The manufacturer-provided table is 32×32 elements in size where each element is a pair of floating-point values (x-axis voltage and y-axis voltage). On its own, this table consumes approximately 8 kbytes of memory which is reasonable, however, we still don't know whether these values will need to be temperature-compensated (i.e. a separate table for each temperature range).

V. FUTURE WORK: FSM TESTBED DEVELOPMENT

Having assessed the device performance against our pointing requirements, the next steps are to repeat this testing in a controlled thermal environment. Although the FSM will be installed in the interior of the CubeSat, it will still experience temperature swings as the satellite goes in and out of eclipse. Additionally, the FSM will be installed in relatively close proximity to the transmitter electronics which represent a significant thermal power source in our design. The expected operating temperature range for the FSM is $0\,°C$ to $40\,°C$.

In order to get a better understanding of the mirror's thermal characteristics, we are developing a testbed capable of driving the mirror with known voltages while measuring the mirror's angular deflection. A schematic of the testbed is shown in Fig. 5 and a photograph of an early prototype is given in Fig. 6. A Raspberry Pi single-board computer has been configured to interface with the MTI PicoAmp FSM driver board. This driver board provides a digital-to-analog converter (DAC) and a high-voltage amplifier capable of generating the $\pm 120\,V$ drive voltages needed by the FSM. A converging 650 nm laser beam reflects from the mirror surface and is focused on a focal plane array (FPA). The focal length of the system and the relative spacing of the lens, FSM and FPA must be carefully selected to avoid unwanted reflections and to maximize the usable resolution of the focal plane array.

The displacement of the spot on the FPA is estimated using a center-of-mass centroiding algorithm and this result is then converted into an angle estimate for the FSM. The FPA that is currently being used in the setup is a monochrome 1280×1024 pixel device with 5.2 µm pixel pitch. Centroiding algorithms typically yield measurement accuracy better than 10% of pixel size. Since the FSM's full range (± 25 mrad) will scan the spot across the entire FPA, we expect to be able to achieve measurement resolutions of approximately 5 µrad.

The testbed is being constructed on a small $30\,cm \times 30\,cm$ optical breadboard that can be installed in a thermal chamber. We plan to "soak" the device at various temperatures across our expected operating temperature range ($0\,°C$ to $40\,°C$). At each temperature level, the 2D transfer function of the FSM will be measured. Additionally, we will perform
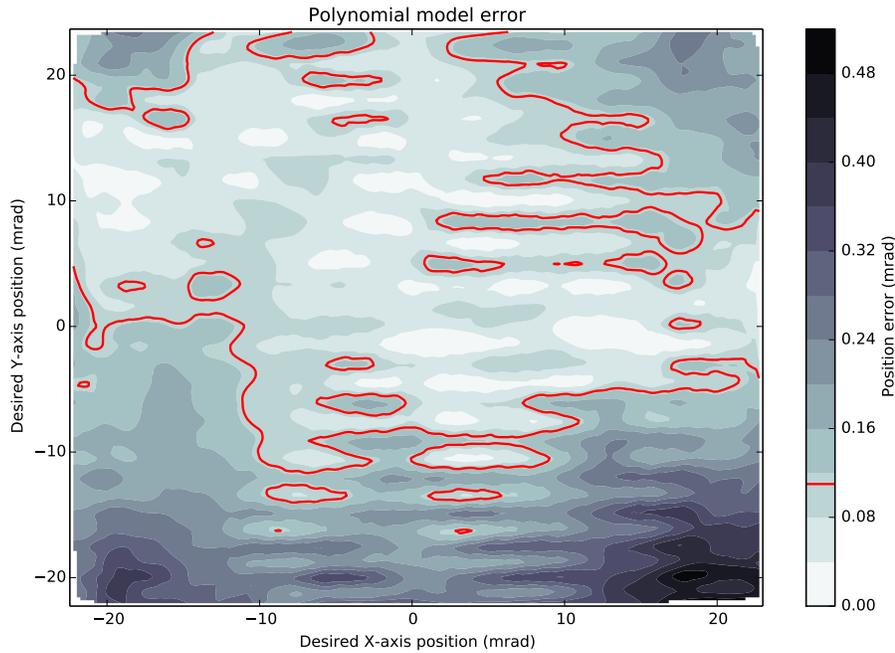
Fig. 4: *Contour plot showing angular error between the polynomial FSM model and measured data. The required performance threshold (± 0.11 mrad) is shown in red.*
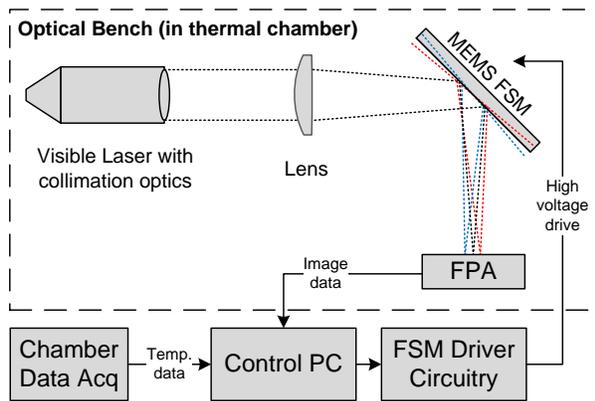
Fig. 5: *Block diagram of the FSM testbed.*
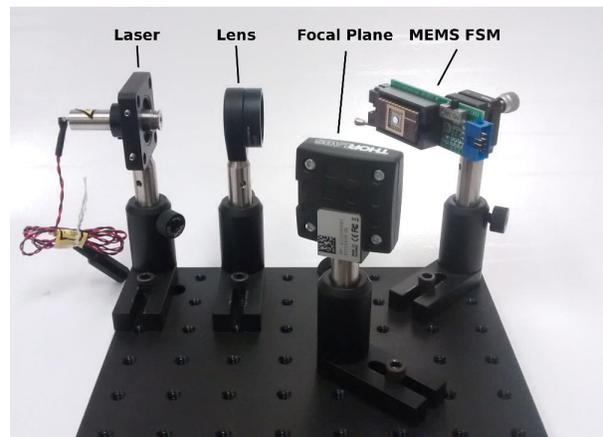
Fig. 6: *Picture of the prototype FSM testbed.*

"repeatability" tests which steer the mirror between predetermined points in repetition. This test will allow us to gather statistics on the pointing uncertainties of the device. There is also some uncertainty about how the testbed assembly (components other than the FSM, e.g. laser, lens and FPA) will be perturbed by the changing thermal environment. To account for this, we will calibrate the rig by performing the above measurements with the FSM unpowered and at rest.

Initial testing will be conducted at 1 atm pressure. We expect to use a hermetically sealed variant of the device for the flight design so testing in vacuum is not a high priority at present.

VI. SUMMARY

We have reviewed commercially-available fine-steering mechanisms for our CubeSat-scale lasercom payload and have selected an electrostatic MEMS device for further development. Analysis of manufacturer-provided device data shows that a 2D lookup table approach will likely be needed to linearize the device. This has memory usage implications for the control processor used in the payload. Our current focus is to develop a testbed that allows us to measure the voltage-to-angle behavior of the mirror. Over the next few months, we expect to use this testbed to characterize the performance of the mirror across our intended operating temperature range.

REFERENCES

[1] R. Kingsbury, K. Riesing, and K. Cahoy, "Design of a free-space optical communication module for small satellites," *Proceedings of the AIAA/USU Conference on Small Satellites*, vol. Session IX: Advanced Technologies-Communication, pp. SSC14–IX–6, 2014.

[2] K. L. Cahoy, A. D. Marinan, B. Novak, C. Kerr, T. Nguyen, M. Webber, G. Falkenburg, and A. Barg, "Wavefront control in space with mems deformable mirrors for exoplanet direct imaging," *Journal of Micro/Nanolithography, MEMS, and MOEMS*, vol. 13, no. 1, pp. 011105–011105, 2014.

[3] B.-W. Yoo, J.-H. Park, I. Park, J. Lee, M. Kim, J.-Y. Jin, J.-A. Jeon, S.-W. Kim, and Y.-K. Kim, "Mems micromirror characterization in space environments," *Optics express*, vol. 17, no. 5, pp. 3370–3380, 2009.

[4] S. Janson and R. Welle, "The NASA optical communication and sensor demonstration program," in *AIAA Small Satellite Conference*, 2013.

[5] E. Peters, P. Davé, R. Kingsbury, M. Prinkey, A. Marinan, E. Wise, C. Pong, K. Cahoy, W. Thalheimer, D. Sklair, *et al.*, "Design and functional validation of a mechanism for dual-spinning cubesats," *AIAA/USU Conference on Small Satellites*, vol. Pre-conference Workshop, 2013.

[6] J. K. Lane, *Control of a MEMS fast steering mirror for laser applications*. PhD thesis, Massachusetts Institute of Technology, 2012.

[7] Mirrorcle Technologies Inc., *Device performance data for 13L2.2 FSM with 2.4mm mirror (S1671)*, Aug 2014.